Real-Solution Stability Diagrams: A Thermodynamic Tool for Modeling Corrosion in Wide Temperature and Concentration Ranges

*A. Anderko, S.J. Sanders, and R.D. Young**

ABSTRACT

A method was developed for construction of stability diagrams for metals in the presence of realistically modeled aqueous solutions. The method was based on a comprehensive thermodynamic model that combines the Helgeson-Kirkham-Flowers (HKF) equation of state for standard-state properties with a solution nonideality model based on the activity coefficient expressions developed by Bromley and Pitzer. Composition-dependent nonideality effects were incorporated into the calculation of predominance areas for dissolved and solid species. Using the combined thermodynamic model, stability diagrams can be computed for systems involving concentrated solutions (i.e., with molalities up to 30 mol/kg) at temperatures up to 573 K and pressures up to 100 MPa. Since the diagrams are based on a realistic thermodynamic model for the aqueous phase, they are referred to as real-solution stability diagrams. In addition to customary potential (E) and pH variables, concentrations of various active species (e.g., complexing agents) can be used as independent variables, making it possible to analyze effects of various compounds that promote or inhibit corrosion. Usefulness of the methodology was demonstrated by generating real-solution stability diagrams for five representative systems (i.e., sulfur-water [S-H_2O], copper-ammonia-water [Cu-NH_3-H_2O], titanium-chlorine-calcium-water [Ti-Cl-Ca-H_2O], iron-sulfur-water (Fe-S-H_2O], and zinc-water [Zn-H_2O]).

KEY WORDS: activity coefficients, complexation, modeling, passivation, solubility, stability diagrams, standard-state properties, thermodynamics

INTRODUCTION

Thermodynamic stability diagrams have been used extensively to predict and rationalize corrosion-related processes since Pourbaix developed a comprehensive collection of diagrams for most elements in water.[1] Pourbaix diagrams depict the areas of thermodynamic stability for various solid or aqueous species as functions of potential (E) and pH. Thus, the diagrams indicate under which E and pH conditions the metal of interest is stable thermodynamically (or immune to corrosion) and which conditions may cause its dissolution in the form of ions or its transformation into metal oxides or other solids that may give rise to passivation. To extend the usefulness of the Pourbaix diagrams, several investigators have developed programs for automatic generation of diagrams.[2-4] Much effort has been focussed on extending the diagrams to high temperatures using the Criss-Cobble[5] correspondence principle for calculating thermochemical properties.[6-10] Several studies have been published on incorporating the effects of dissolved chloride and sulfide ions[6,8] and organic complexing agents.[11]

However, there is still room for improved thermodynamic tools for corrosion modeling because currently available stability diagrams are subject to some inherent limitations. First, the classical stability diagrams have been constructed for arbitrarily assumed activities of dissolved species because of difficulties in developing predictive activity coefficient models for multicomponent solutions. Without a comprehensive activity coefficient model, it is only

Submitted for publication October 1995; in revised form, February 1996.

* OLI Systems Inc., 108 American Road, Morris Plains, NJ, 07950.

0010-9312/97/000011/$5.00+$0.50/0

possible to use numerical values of activity coefficients that correspond to a solution of well-known composition, such as seawater.[12] The absence of an activity coefficient model limits accuracy of the diagrams to very dilute solutions, for which the assumed activities can be identified with concentrations. Another limitation is that pH is introduced as an independent variable without regard to the chemical identity of the sources of the hydrogen (H^+) and hydroxyl (OH^-) ions, which determine pH. Additionally, the classical diagrams are restricted to E and pH as independent variables, whereas it is frequently of interest to analyze effects of species other than H^+ or OH^- ions. For example, it might be worthwhile to use concentrations of complexing species as independent variables. Also, it often is more convenient to consider pH as a dependent rather than independent variable because it results from the presence of various acidic or basic components whose concentrations may be more natural as independent variables.

In the present work, a methodology is proposed to overcome these limitations with the help of a comprehensive thermodynamic model that makes it possible to achieve the following goals:

— Incorporation of an activity coefficient model for multicomponent systems;

— Application to concentrated solutions (i.e., for ionic strengths up to 30 mol/kg);

— Application over extended temperature (T) and pressure (P) ranges (i.e., for T up to 573 K and P up to 100 MPa).

— Flexibility with respect to the choice of independent variables so that the effect of any solution components can be studied explicitly; and

— Use of realistically modeled acids and bases to vary solution pH.

Since the diagrams are based on a realistic model for the aqueous phase, they are referred to as real-solution stability diagrams.

THERMODYNAMIC MODEL

For realistic modeling of multicomponent, multiphase electrolyte systems, a comprehensive thermodynamic model is of utmost importance. The model must combine information about standard-state properties of all species present in the system with accurate formulation for the excess Gibbs energy, which accounts for the solution nonideality. Additionally, it must be coupled with an efficient algorithm for calculating phase equilibria in multicomponent systems that may contain an aqueous phase, any number of solid phases, a vapor phase, and/or a nonaqueous liquid phase. These conditions are satisfied by the thermodynamic model that forms the basis of an aqueous simulation technology that has been developed previously by OLI Systems Inc. This model has been described in detail by Zemaitis, et al.,[13] and Rafal, et al.[14] In this work, the essential elements of the model are outlined to explain how it can be used to generate real-solution stability diagrams.

In a multicomponent system, the partial molal Gibbs energy of the i-th species ($\bar{G}_i$) is related to the molality (m_i) by:

$$\bar{G}_i = \bar{G}_i^0 + RT \ln_i \gamma_i \qquad (1)$$

where $\bar{G}_i^0$ is the standard-state partial Gibbs energy, and γ_i is the activity coefficient. Thus, thermodynamic properties of the system can be calculated if the standard-state Gibbs energies are available for all species as functions of T and P (i.e., $\bar{G}_i^0$ [T, P]), and the activity coefficients are known as functions of the composition vector m and T (i.e., γ_i[m, T]). From basic thermodynamics, the standard-state Gibbs energy of formation ($\bar{G}_i^0$ [T, P]) can be calculated as a function of T and P if the following data are available: the Gibbs energy of formation at a reference temperature and pressure (usually, T_r = 298.15 K and P_r = 0.1 MPa), enthalpy of formation at T_r and P_r, entropy at T_r and P_r, heat capacity as a function of T and P, and volume as a function of T and P.

The key to representing the standard-state properties over substantial T and P ranges is accurate knowledge of the heat capacity and volume. Traditionally, Pourbaix diagrams for systems at elevated temperatures[6-10] were constructed by using the entropy correspondence principle of Criss and Cobble[5] to calculate the temperature dependence of standard-state properties of ions, whereas the pressure dependence was neglected. In this work, the Helgeson-Kirkham-Flowers (HKF) equation of state for standard-state properties was used.[15-17] This equation accurately represents the standard-state thermodynamic functions for aqueous, ionic, or neutral, species as functions of T (up to 1,273 K) and P (up to 500 MPa).

The HKF equation expresses heat capacity and volume as functions of pure water properties and seven empirical parameters, which have been calculated for large numbers of ions, complexes and neutral, inorganic and organic, molecules.[18-21] The remaining thermodynamic properties are obtained by thermodynamic integration using values of the Gibbs energy, enthalpy, and entropy at T_r and P_r as integration constants. Numerical values of the HKF equation parameters are collected in the papers of Shock, et al.,[18-21] and Rafal, et al.[14] If the HKF equation parameters are not available from the regression of experimental data, they can be estimated. For this purpose, correlations have been developed for simple species as well as complexes between metals and various ligands.[19-20,22] These and other estimation techniques have been reviewed in detail by Rafal, et al.[14]

The activity coefficient model used for representing solution nonideality is an extended form of an expression developed by Bromley.[23-24] The Bromley equation is a combination of the Debye-Hückel term for long-range electrostatic interactions and a semiempirical expression for short-range interactions between cations and anions.[25] In a multicomponent system, the activity coefficient of an ion i is given by:

$$\log \gamma_i = \frac{-Az_i^2 I^{1/2}}{1 + I^{1/2}} + \sum_j^{NO} \left[\frac{|z_i| + |z_j|}{2} \right]^2 \left[\frac{(0.06 + 0.6\, B_{ij}) |z_i z_i|}{\left(1 + \frac{1.5}{|z_i z_j|} I\right)^2} + B_{ij} + C_{ij}\, I + D_{ij}\, I^2 \right] m_j \quad (2)$$

where A is the Debye-Hückel coefficient, which depends on temperature and solvent properties;[13] z_i is the number of charges on ion i; I is the ionic strength (i.e., $I = 0.5\sum z_i^2 m_i$); NO is the number of ions with charges opposite to that of ion i; and B_{ij}, C_{ij} and D_{ij} are empirical, temperature-dependent, cation-anion interaction parameters. Bromley's original formulation contains only one interaction parameter, B_{ij}, which is sufficient for systems with moderate ionic strength. For concentrated systems, the additional coefficients C_{ij} and D_{ij} usually become necessary. The three-parameter form of the Bromley model is capable of reproducing activity coefficients in solutions with ionic strength up to 30 mol/kg. Temperature dependence of the B_{ij}, C_{ij}, and D_{ij} parameters usually is expressed using a simple quadratic function. These parameters are obtained by regressing experimental solubility and vapor-liquid equilibrium data. In the absence of experimental data, B_{ij} can be estimated from contributions of individual ions:

$$B = B_+ + B_- + \delta_+ \delta_- \quad (3)$$

where B_+ and δ_+ are constants for a specific cation and B_- and δ_- are constants for a specific anion. In turn, the B_+ and B_- contributions can be predicted using a correlation with the entropy of ions:

$$B_i = a_i \bar{S}_i^0 + b_i \quad (4)$$

where B_i is either B_+ or B_-, a_i and b_i are coefficients specific for an ion class under consideration, and $\bar{S}_i^0$ is the standard-state entropy at T_r and P_r. When Equation (4) is used, the correction terms δ_+ and δ_- are assumed to be equal to zero. A method by Meissner makes it possible to extrapolate the activity coefficients to higher ionic strengths based on only a single experimental or predicted data point.[26]

The Bromley model is restricted to interactions between cations and anions. For ion-molecule and molecule-molecule interactions, the model of Pitzer is convenient.[27] Unlike the Bromley model, the Pitzer model is not accompanied by methods for estimating missing parameters. Thus, application of the Pitzer model always is based on regression of available experimental data. However, reasonable predictions can be obtained from the Bromley model even when no parameters were regressed previously as long as cation-anion interactions are predominant in the system of interest.

The combined thermodynamic model is valid for T up to 573 K, P up to 100 MPa and compositions up to 30 m. For individual systems, the range of high accuracy may be limited due to a lack of experimental data for parameter regression (especially solution nonideality data) and, therefore, a greater dependence on the estimation of parameters. The model is supported by an extensive data bank that covers the majority of existing inorganic species and a substantial number of organic species.

CONSTRUCTION OF REAL-SOLUTION STABILITY DIAGRAMS

A stability diagram for a given physical system can be viewed as a superposition of elementary diagrams for the redox subsystems that make up the system of interest. For example, a system composed of an iron-nickel (Fe-Ni) alloy in a hydrogen sulfide (H_2S) solution can be treated as a superposition of five redox subsystems defined as:

— All species containing Fe in any possible oxidation state (0, +2, +3, and, possibly, +6);

— All species with Ni in the 0, +2, +3, and +4 oxidation states;

— All species with sulfur (S) in any possible oxidation state ranging from –2 to +8;

— All species with H in the 0 and +1 oxidation state; and

— All species with oxygen (O) in the –2, 0, and, possibly, –1 oxidation states.

Thus, each redox subsystem is associated with an element that can exist in two or more oxidation states. Each of the elementary redox subsystems is characterized by a set of reactions that may occur between the species that belong to the subsystem. The subsystems are interdependent because the reactions in each subsystem involve species that belong to more than one subsystem. However, the relationships between the potential and activities or concentrations of species can be plotted separately for each subsystem. The classical Pourbaix diagrams are shown as superpositions of three elementary diagrams (i.e., one for a redox subsystem containing a selected metal, one for the oxygen subsystem and one for the hydrogen subsystem). The latter two sub-

systems usually are represented by single lines that correspond to the H^+/H_2 and O_2/H_2O equilibria.

To compute a stability diagram for each redox subsystem, it is necessary to enumerate all distinct chemical species that belong to this subsystem. Each of these species contains the particular element that is associated with the subsystem. Then, equilibrium equations are written between all species in the subsystem. If the number of species is n, then n(n – l)/2 reactions are defined. A reaction between the species X and Y is written as:

$$\nu_x X + \sum_{i=1}^{k} \nu_i A_i = Y + \nu_e e^- \quad (5)$$

where A_i (i = 1,..., k) are the basis species necessary to define equilibrium equations between all species in the redox subsystem and ν_i are the stoichiometric coefficients. For convenience, each reaction is normalized so that the stoichiometric coefficient for the right-hand side species (Y) = 1.

To establish a general algorithm for defining the basis species A_i, the species X and Y from Equation (5) can be represented as:

$$X \equiv M_{X_1} H_{X_2} O_{X_3} C_{X_4} D_{X_5} E_{X_6} \ldots \quad (6)$$

$$Y \equiv M_{Y_1} H_{Y_2} O_{Y_3} C_{Y_4} D_{Y_5} E_{Y_6} \ldots \quad (7)$$

where M is the element that is associated with the redox subsystem; H and O are the usual symbols for hydrogen and oxygen; and C, D, E, ... are the additional elements that exist in the species X and Y. For the purpose of defining the basis species, elements in different oxidation states are treated separately. For example, C and D can represent the same element in two different oxidation states. The basis species then are defined as the species that contain H, O, C, D, and E, etc., but that do not contain M. Although this definition allows considerable flexibility in choosing the basis species A_i, additional rules are introduced to simplify the algorithm:

— H^+ is always the basis species that contains H;

— H_2O is always the basis species that contains O; and

— The basis species containing C, D, and E, etc. are selected so that they contain the minimum possible number of hydrogen and oxygen atoms in addition to C, D, and E ....

To illustrate the selection of basis species, two examples are considered. In a system composed of copper (Cu), H_2O, and ammonia (NH_3), the species in the Cu-containing redox subsystem are copper hydroxides, oxides, and complexes formed by Cu with the OH and NH_3 groups. Therefore, the general formula for the species is $Cu_{X_1} H_{X_2} O_{X_3} N_{X_4}^{-3}$ where N^{-3} denotes N in the –3 oxidation state. Thus, the basis species for constructing Reaction (5) are H^+, H_2O, and $NH_{3(aq)}$. In a system composed of Fe, H_2O, and S-bearing compounds, the species in the Fe subsystem are iron hydroxides, oxides, hydroxycomplexes, sulfides, polysulfides, and sulfates. The general formula for the species is $Fe_{X_1} H_{X_2} O_{X_3} S_{X_4}^{-2} S_{X_5}^{0} S_{X_6}^{+6}$, and the basis species are H^+, H_2O, S^{2-}, $S^0_{(s)}$, and SO_4^{2-}.

After selecting the basis species, the stoichiometric coefficients in Equation (5) are determined by balancing the elements M, H, O, C, D, and E, etc. Finally, the number of electrons (ν_e) is found by balancing the charges on the right- and left-hand sides of Equation (5).

The selection of basis species is slightly more complicated in cases when not only the element M (Equations [6] and [7]) is subject to redox equilibria, but also when some of the elements C, D, and E, etc. can enter into their own redox equilibria. A typical example is the Fe-H_2O-S system, in which both Fe and S can exist in several oxidation states. In the Fe-containing subsystem, the transformations between the various $Fe_{X_1} H_{X_2} O_{X_3} S_{X_4}^{-2} S_{X_5}^{0} S_{X_6}^{+6}$ species can involve oxidation and reduction of Fe or S or both. In such cases, the basis species are modified in a two-step procedure:

— First, it is determined which basis species are stable in which area of the stability diagram; and

— Second, only the stable species are retained in the basis, and the remaining ones are deleted. The deleted species are not taken into account in constructing the equilibrium Equation (5). Otherwise, they are kept in the system.

Since different basis species can be stable in various areas of a stability diagram, the two steps usually are repeated in as many areas of the diagram as necessary. This procedure ensures that only the stable basis species are included in the reactions. For example, elemental sulfur (S^0) is stable only in a certain fraction of the E-vs-pH plane. Therefore, S^0 is used as a basis species to construct the reactions for the Fe subsystem only when S^0 is stable (i.e., when solid S can exist in a finite amount).

The proposed procedure for constructing equilibrium equations is considerably more complicated than techniques proposed in the literature in conjunction with the classical Pourbaix diagrams.[1] However, this procedure makes it possible to include chemical transformations of any complexity and is not limited to those involving H^+ and H_2O.

Equilibrium Lines

In the classical Pourbaix diagrams, each line represents the equilibrium between two chemical species for a given activity. Since the activity of dissolved species is assumed a priori, it is possible to derive analytical expressions for the equilibrium lines. Such expressions give pH values for the equilibrium between two species that do not undergo a

redox reaction and express the potential as a linear function of pH for redox transformations. In the real-solution stability diagrams, activities of all species vary because of the changing amounts of input species (such as an acid or a base used to adjust pH). Activity coefficients are nonlinear functions of composition and may cause nonlinearities in the equilibrium lines. Therefore, it is not possible to derive analytical expressions for the equilibrium lines. Instead, a certain number of points on the equilibrium lines must be computed numerically. The points can be interpolated further to obtain an equilibrium line.

Stability diagrams are constructed by performing a simulated titration with reactants that are appropriate for varying the independent variable of interest. If pH is the independent variable, two reactants — an acid and a base — are selected for the simulated titration. First, decreasing amounts of an acid are added to cover the acidic pH range in regular increments. Then, increasing amounts of a base are added to cover the basic pH range. If the influence of a complexing or other reactive species is studied, the input amount of this species or its equilibrium concentration can be chosen as possible independent variables. Then, a compound containing this species is added in regular increments. For each amount of the added reactant, equilibrium compositions of various species in the aqueous phase are computed. For this purpose, appropriate mass balance and electroneutrality conditions also must be taken into account.[13-14] At the same time, the activity coefficients are obtained. The concentrations and activity coefficients are used to calculate the points on the equilibrium lines. In typical diagrams, it is sufficient to calculate between 20 and 30 points on the equilibrium lines provided that they are evenly spaced to cover a full range of the selected independent variable.

Chemical Reactions

The chemical reactions are defined as the ones for which ν_e (Equation [5]) is zero. Since the chemical reactions are independent of the potential, they are represented on stability diagrams as vertical lines. In this case, an equation for the affinity A of Reaction (5) is written as:

$$\frac{A}{RT} = -\frac{1}{RT}\left(\bar{G}_Y - \nu_X\bar{G}_X - \sum_{i=1}^{k}\nu_i\bar{G}_{A_i}\right) = \ln K - \left(a_Y - \nu_X \ln a_X - \sum_{i=1}^{k}\nu_i \ln a_{A_i}\right) \quad (8)$$

where K is the equilibrium constant of Reaction (5) and a_i denotes the activity of species i. The equilibrium constant is calculated from the standard-state Gibbs energies $\bar{G}_i^0$ as:

$$\ln K = \frac{1}{RT}\left(\bar{G}_Y^0 - \nu_X\bar{G}_X^0 - \sum_{i=1}^{k}\nu_i\bar{G}_{A_i}^0\right) \quad (9)$$

The activities of dissolved species are related to the molalities m_i and activity coefficients γ_i by:

$$a_i = m_i\gamma_i \quad (10)$$

At equilibrium, the affinity of the reaction is equal to zero. In the particular case when Reaction (5) occurs between an aqueous and a solid species, the equilibrium corresponds to the precipitation of an infinitesimal amount of the solid phase. If Reaction (5) is between two aqueous species, the point of zero affinity corresponds to equal activities of the species X and Y. If the affinity is positive, the species on the right side of Equation (5) predominates. Similarly, if the affinity is negative, the species on the left side is predominant. The species that is not predominant may be absent completely (which is usually the case for precipitation equilibria) or may be present in smaller quantities than the predominant species.

The values of the affinity of the chemical reaction (Equation [8]) are calculated for each step of the simulated titration. This allows construction of a discrete function:

$$A_p = f\left(var_p\right) \quad p = 1, \ldots, N \quad (11)$$

where var_p is the independent variable (such as pH or concentration of a complexing agent) at the point p of the simulated titration, A_p is the corresponding value of the affinity of Reaction (8), and N is the total number of steps in the simulated titration. The function $f(var_p)$ of Equation (11) then is interpolated using cubic splines. The interpolating function is used to find the independent variable var_0, for which A = 0:

$$f\left(var_0\right) = 0 \quad (12)$$

The independent variables found in this way are later used as the coordinates of the vertical lines on the stability diagram. After finding the root of Equation (12), it is necessary to check which one of the two species is more stable at var > var_0 and at var < var_0. This is accomplished easily by checking the sign of the function f(var). For particular pairs of species, the root of Equation (12) may not be found, which means that one of the species is more stable in the entire range of independent variables. The analysis of chemical equilibrium equations is repeated for each pair of species, for which ν_e is zero. Thus, a collection of vertical boundaries in the stability diagram is established.

Electrochemical Reactions

In the case of electrochemical reactions, ν_e in Equation (5) is not equal to zero. In this case, equilibrium potentials that correspond to Reaction (5) are computed for each pair of species X and Y:

$$E = E^0 + \frac{RT}{F\nu_e}\left(\ln a_Y - \nu_X \ln a_X - \sum_{i=1}^{k} \nu_i \ln a_{A_i}\right) \qquad (13)$$

where R is the gas constant, F is the Faraday constant, and E^0 is related to the standard-state Gibbs energies by:

$$E^0 = \frac{\bar{G}_Y^0 - \nu_X \bar{G}_X^0 - \sum_{i=1}^{k} \nu_i \bar{G}_{A_i}^0}{F\nu_e} \qquad (14)$$

Values of the potential are obtained from Equations (13) and (14) for each step of the simulated titration and used to construct a discrete function of the independent variable:

$$E_p = g\left(var_p\right) \qquad p = 1, \ldots, N \qquad (15)$$

where var_p is the independent variable at the point p of the simulated titration, and E_p is the value of the potential calculated from Equation (13). The function of Equation (15) then is interpolated using cubic splines.

Areas of Predominance

After determining the equilibrium lines that correspond to chemical and electrochemical equilibria, areas of predominance are computed for each species in the redox subsystem of interest. For each species, four classes of boundaries are differentiated:

— Upper boundaries, which correspond to equilibria with other species that are in higher oxidation states. If ν_e in Equation (5) is positive, the line determined by Equation (13) will be an upper boundary for the species X. Conversely, if $\nu_e < 0$, the line determined by Equation (13) will be an upper boundary for the species Y.

— Lower boundaries, which correspond to equilibria with other species that are in lower oxidation states. The line determined by Equation (13) will be a lower boundary for the species X if $\nu_e < 0$ or a lower boundary for Y if $\nu_e > 0$.

— Right-hand side boundaries, which mean that the species under consideration is predominant for independent variables that are lower than the root var_0 of Equation (12).

— Left-hand side boundaries, which mean that the species is predominant for independent variables that are greater than var_0. The sign of the affinity (Equation [11]) is used to determine whether a vertical boundary is a right- or left-hand side boundary.

In general, there can be several boundaries of each kind. Therefore, an automatic procedure is set up to find intersection points between the boundaries and determine which ones are active (e.g., the lowest upper boundary and the highest lower boundary will be active for any given independent variable). In the case of systems in which the basis species are adjusted depending on the stability of the potential ligands, the stability areas of the ligands are determined prior to calculation of the predominance areas for the redox subsystem of interest. Then, the predominance areas for the redox subsystem are determined separately within the stability area of each ligand. Despite the separate determination of the predominance areas in different parts of the diagram, there is always a smooth transition at the boundaries between the ligand stability areas because the reaction equilibria, concentrations, and activity coefficients in each ligand stability area are interdependent and mutually consistent.

Although the procedure for calculating the equilibrium lines is entirely different from that used for the classical Pourbaix diagrams, the determination of predominance areas from previously computed equilibrium lines is similar to that described in previous works.[2-3] The main difference is that predominance areas in a classical Pourbaix diagram can be constructed as convex polygons, whereas those in the real-solution stability diagrams can have curved boundaries and do not have to be convex. This is because the equilibrium lines for electrochemical reactions are not necessarily represented by straight lines.

VERIFICATION OF THE THERMODYNAMIC MODEL

The accuracy of the thermodynamic model used in this work has been verified extensively by Zemaitis, et al.,[13] and Rafal, et al.[14] In the present work, the model was verified additionally for two aqueous systems (i.e., $NH_3 + H_2O$ and zinc oxide [ZnO] + potassium hydroxide [KOH] + H_2O) simulated in this study in conjunction with generating sample stability diagrams. The best way to verify the accuracy of an activity coefficient model is to compare the predicted solubilities of solids (i.e., solid-liquid equilibria) and equilibrium total and partial pressures (i.e., vapor-liquid equilibria) with experimental data.

Figure 1 compares the predicted total pressures as well as NH_3 partial pressures in the NH_3-H_2O system with experimental data. As shown in Figure 1, the model accurately represents the vapor-liquid equilibria[28] for NH_3 molalities up to 30 mol/kg. Figure 2 shows the solubility relationships in the ternary ZnO-KOH-H_2O system.[29] Since the solids in

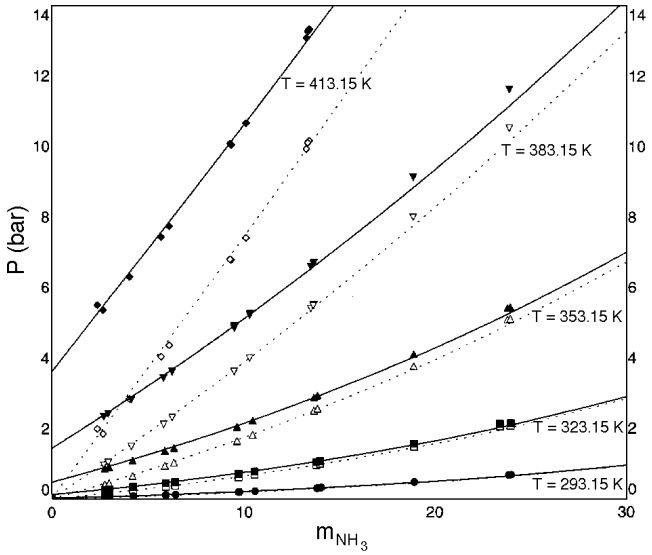

FIGURE 1. *Representation of vapor-liquid equilibria in the NH_3-H_2O system. Solid and dotted lines show the calculated total pressure and partial pressure of NH_3, respectively. Solid and hollow symbols denote the experimental total and partial pressures, respectively.[28]*

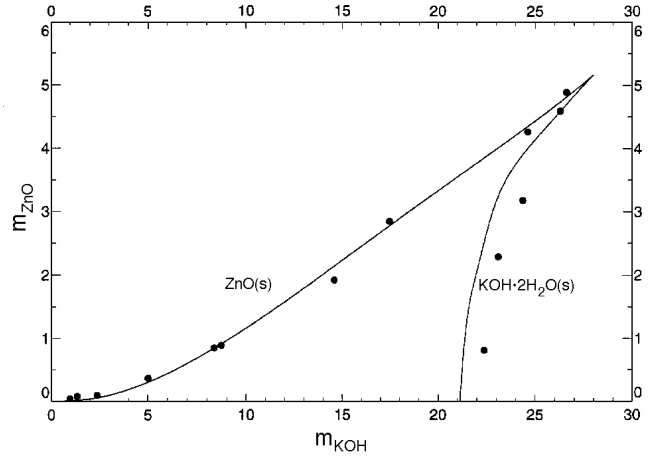

FIGURE 2. *Solubility of ZnO and KOH·2H_2O in the ternary system H_2O + KOH + ZnO at 298.15 K. Solid lines show results obtained from the thermodynamic model . Circles denote the data of Dirkse.[29]*

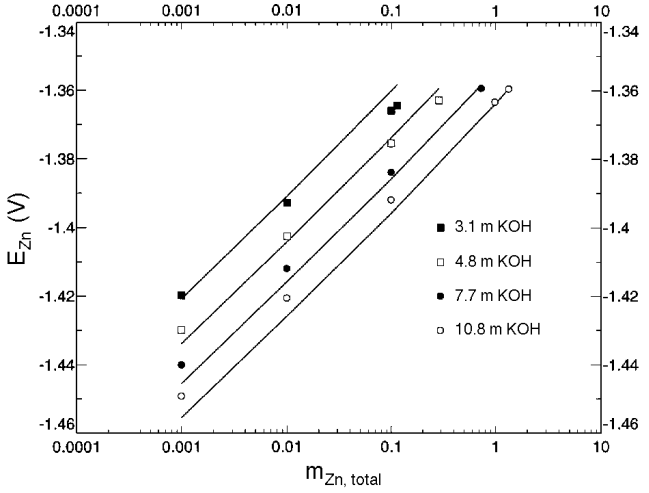

FIGURE 3. *Zn electrode rest potentials at 298.15 K vs Hg-HgO predicted using the thermodynamic model (solid lines) and measured (symbols) by Isaacson, et al.[30]*

this system are easily soluble, the ionic strength reaches 30 mol/kg. In such concentrated solutions, solubilities are very sensitive to activity coefficients. In contrast to the NH_3-H_2O system, the liquid-phase nonideality in the ZnO-KOH-H_2O system is determined by cation-anion interactions. The most important binary interaction is between the K^+ and $Zn(OH)_4^{2-}$ ions because $Zn(OH)_4^{2-}$ is the predominant zinc (Zn) species in highly alkaline solutions. As shown in Figure 2, the solubility of ZnO in KOH is reproduced within experimental error. Small deviations from the data are noted only for the solubility of KOH·2H_2O, which also can precipitate in this system.

Additionally, the thermodynamic model can be verified by comparing the calculated rest potentials of the Zn electrode in concentrated KOH + ZnO solutions with experimental data obtained by Isaacson, et al.,[30] vs the mercury-mercuric oxide (Hg-HgO) electrode. In view of the predominance of the $Zn(OH)_4^{2-}$ ion, the overall cell reaction is Zn + $2OH^-$ + HgO + H_2O = $Zn(OH)_4^{2-}$ + Hg. Thus, the cell potential can be predicted because the activities of all solution species (i.e., $Zn[OH]_4^{2-}$, OH^-, and H_2O) can be obtained easily from equilibrium calculations as functions of the input amounts of KOH and ZnO:

$$E = \frac{\bar{G}^0_{Zn(OH)_4^{2-}} - 2\bar{G}^0_{OH^-} - \bar{G}^0_{HgO}}{2F} + \frac{RT}{2F} \ln \frac{a_{Zn(OH)_4^{2-}}}{a^2_{OH^-} a_{H_2O}} \qquad (16)$$

The predicted potentials are shown in Figure 3 for various composition of the system. Although the rest potential data were not used for regressing the interaction parameters, the agreement is very satisfactory, and the average deviation from experimental data is 0.27%. Thus, it could be concluded that the thermodynamic model accurately represents the equilibrium properties of concentrated solutions containing ions and neutral species.

APPLICATION EXAMPLES

To examine the characteristics of the real-solution stability diagrams, five representative systems that are of interest for corrosion simulation were studied: S-H_2O, Cu-NH_3-H_2O, titanium-chlorine-calcium-water (Ti-Cl-Ca-H_2O), Fe-S-H_2O, and Zn-H_2O. All possible aqueous, solid, and gaseous species were taken into account provided that their thermody-

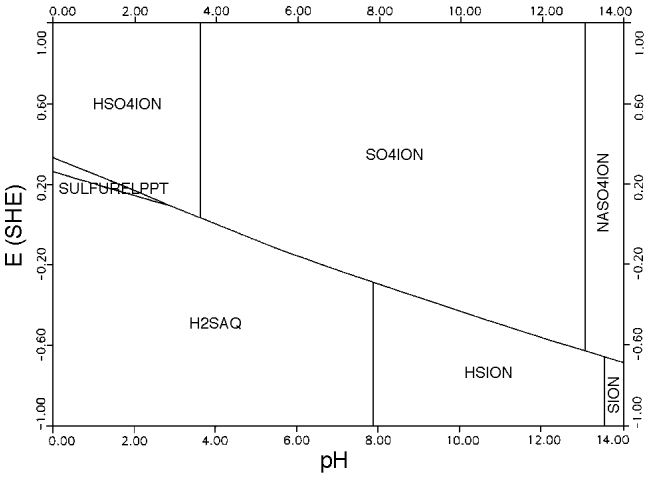

FIGURE 4. *Stability diagram for a system containing 0.01 mol H_2S in 1 kg of H_2O with H_2SO_4 and NaOH used as pH-adjusting agents (T = 298.15 K, P = 1 bar). The symbols HSO4ION, SO4ION, NASO4ION, SULFURELPPT, H2SAQ, HSION, and SION denote HSO_4^-, SO_4^{2-}, $NaSO_4^-$, $S_{(s)}$, $H_2S_{(aq)}$, HS^-, and S^{2-}.*

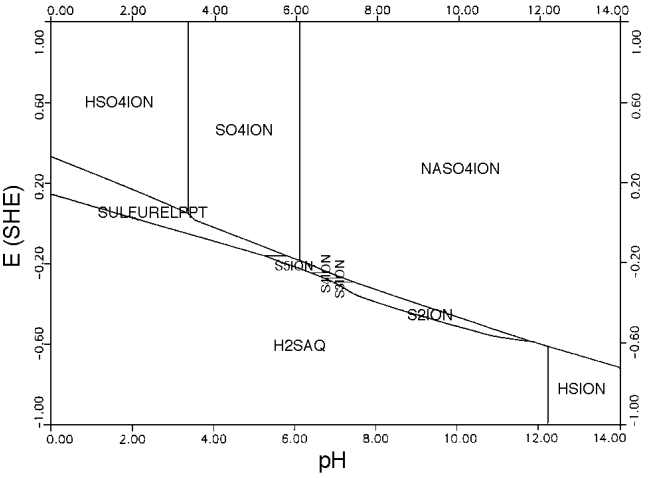

FIGURE 5. *Stability diagram for a system containing 5 mol H_2S in 1 kg of H_2O with H_2SO_4 and NaOH used as pH-adjusting agents (T = 298.15 K, P = 10 bar). The symbols HSO4ION, SO4ION, NASO4ION, SULFURELPPT, S5ION, S4ION, S3ION, S2ION, H2SAQ, and HSION denote HSO_4^-, SO_4^{2-}, $NaSO_4^-$, $S_{(s)}$, S_5^{2-}, S_4^{2-}, S_3^{2-}, S_2^{2-}, $H_2S_{(aq)}$, and HS^-.*

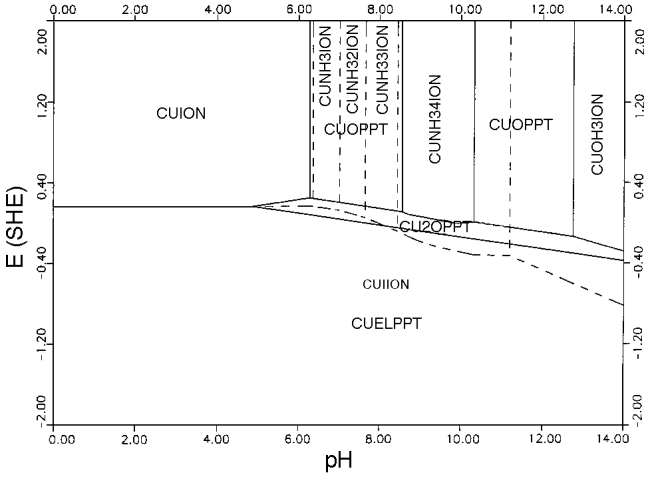

FIGURE 6. *Stability diagram for Cu in a 1 molal NH_3 solution with H_2SO_4 and NaOH used as pH-adjusting agents (T = 298.15 K, P = 1 bar). The symbols CUION, CUIION, CUNH3ION, CUNH32ION, CUNH33ION, CUNH34ION. CUOPPT, CU2OPPT, CUOH3ION, and CUELPPT denote Cu^{2+}, Cu^+, $CuNH_3^{2+}$, $Cu(NH_3)_2^{2+}$, $Cu(NH_3)_3^{2+}$, $Cu(NH_3)_4^{2+}$, $CuO_{(s)}$, $Cu_2O_{(s)}$, $Cu(OH)_3^-$, and $Cu_{(s)}$.*

namic properties were available in the literature or could be estimated using the methods discussed. Results are shown in Figures 4 through 12. The names of the species in Figures 4 through 12 are followed by the suffixes -ION, -AQ and -PPT, which denote an ion, a neutral aqueous species, and a solid (precipitate), respectively. Symbols of individual elements that may exist in more than one oxidation state are followed by their oxidation states expressed by Roman numerals. For example, FEII, FEIII, and TIIV denote Fe(II), Fe(III), and Ti(IV), respectively.

Elements are identified by the abbreviation EL. For example, solid elemental Fe is denoted by FEELPPT, where FE identifies iron, EL represents an element (oxidation state of zero), and PPT denotes a solid.

Figures 4 and 5 illustrate the effect of concentrations of active species on the stability diagram of the relatively simple S + H_2O system. Figure 4 was generated for a system obtained by equilibrating 0.01 mol of H_2S with 1 kg of H_2O at 298.15 K and 0.1 MPa. The pH was varied by adding sulfuric acid (H_2SO_4) and sodium hydroxide (NaOH) to the solution. In view of the small overall concentration of S^1 in this system (i.e., 0.01 mol/kg), the solution is only slightly nonideal. Therefore, the obtained diagram is almost identical to the classical Pourbaix diagram for S. The only difference is the presence of the $NaSO_4^-$ ion at high pH values, which is a consequence of adding NaOH to obtain alkaline solutions.

The diagram appreciably changes when the input amount of H_2S is increased to 5 mol/kg, and the pressure is set at 1 MPa, thus creating a more concentrated solution (Figure 5). The increase in the overall amount of S causes the appearance of areas in which the polysulfide ions S_2^{2-}, S_3^{2-}, S_4^{2-}, and S_5^{2-} predominate. Similarly to the $S_{(s)}^0$ stability area, the polysulfide areas are between those for S in the –2 and +6 oxidation states. Unlike elemental sulfur, the polysulfides are stable in neutral and alkaline solutions. The polysulfide solutions are characterized by the existence of several ions (i.e., S_2^{2-}, S_3^{2-}, S_4^{2-}, S_5^{2-}, HS^-, and $H_2S_{(aq)}$) in equilibrium. The equilibrium between them is a sensitive function of solution alkalinity, the overall concentration of S, and the total concentration of zero-valent S. Therefore, the

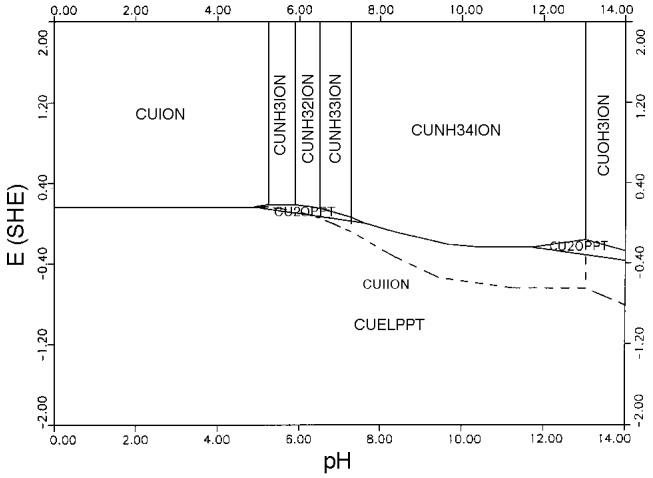

FIGURE 7. *Stability diagram for Cu in a 1 molal NH_3 solution with H_2SO_4 and NaOH used as pH-adjusting agents (T = 298.15 K, P = 1 bar). The symbols CUION, CUIION, CUNH3ION, CUNH32ION, CUNH33ION, CUNH34ION, CU2OPPT, CUOH3ION, and CUELPPT denote Cu^{2+}, Cu^{+}, $CUNH_3^{2+}$, $CU(NH_3)_2^{2+}$, $CU(NH_3)_3^{2+}$, $CU(NH_3)_4^{2+}$, $CU_2O_{(s)}$, $CU(OH)_3^{-}$, and $CU_{(s)}$.*

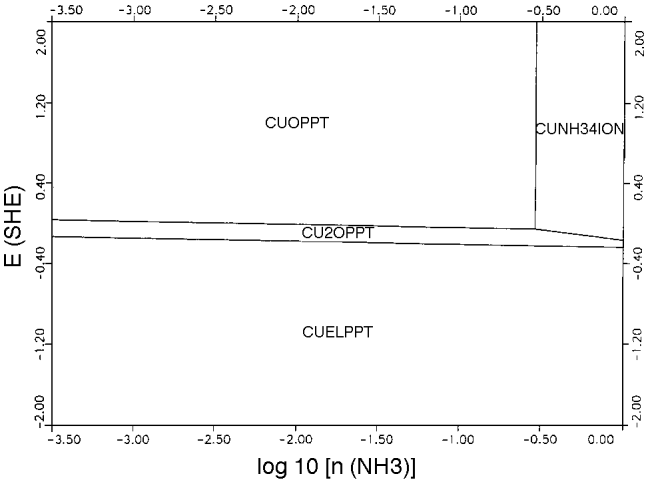

FIGURE 8. *Stability diagram for Cu in a solution with varying concentration of NH_3 (from 0.00032 to 1 molal) at T = 298.15 K and P = 1 bar. The symbols CUNH34ION, CU2OPPT, CUOPPT, and CUELPPT denote $Cu(NH_3)_4^{2+}$, $Cu_2O_{(s)}$, $CuO_{(s)}$, and $Cu_{(s)}$.*

location of the boundaries between the predominance fields of polysulfide species is influenced significantly by the values of activity coefficients. The effect of solution nonideality manifests itself in the curved boundaries between S_2^{2-} and H_2S as well as S^0 and SO_4^{2-} (Figure 5).

An important feature of the real-solution stability diagrams is their usefulness for analyzing the effects of various complexing agents. This is illustrated in Figures 6 through 8 for the Cu + NH_3 + H_2O system. As shown by Pourbaix, the stability diagram for Cu in water without NH_3 includes large predominance areas of CuO and Cu_2O, which are responsible for the passivation of Cu in oxidizing environments. The addition of NH_3 substantially affects the stability of the passivating oxides CuO and Cu_2O because of the formation of several complexes (i.e., $Cu[NH_3]_i^{2+}$ where i = 1,...,5). The complexes are stable in the intermediate range of pH values, which coincides with the stability ranges of CuO and Cu_2O. If the input molality of NH_3 in the solution is 0.1, the stability field of CuO splits into two separate areas (Figure 6). Between these two areas, CuO is unstable because it is superseded by the soluble complex $Cu(NH_3)_4^{2+}$. Figure 7 shows the behavior of this system when the input amount of NH_3 is increased to 1 mol/kg. In this case, CuO becomes unstable in the entire pH range. Also, the stability of Cu_2O is reduced to two small separate areas in nearly neutral and alkaline solutions.

It is worthwhile to examine the amount of NH_3 that causes the disappearance of the copper oxide stability fields. For this purpose, it is convenient to replace pH with the input amount of NH_3 as an independent variable. Figure 8 shows a projection of E vs

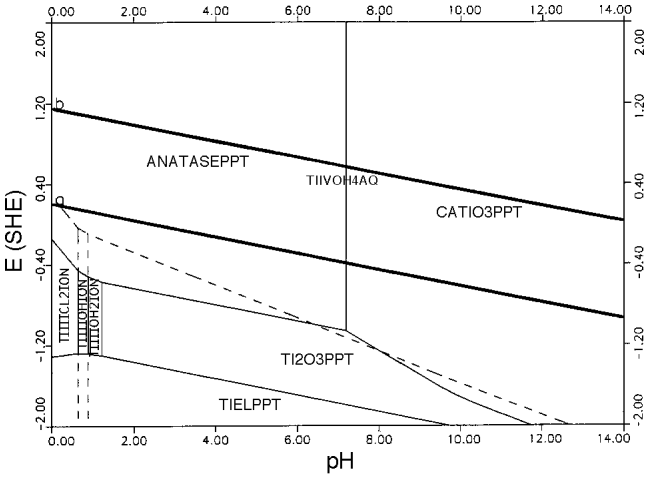

FIGURE 9. *Stability diagram for Ti in a 0.01 molal calcium hydroxide ($Ca[OH]_2$) solution with hydrochloric acid (HCl) and NaOH used as pH-adjusting agents (T = 413.15 K, P = 10 bar). The symbols TIIVOH4AQ, TIIIICL2ION, TIIIIOHION, TIIIIOH2ION, ANATASEPPT, CATIO3PPT, TI203PPT, and TIELPPT denote $Ti(OH)_{4(aq)}$, $TiCl_2^{+}$, $Ti(OH)^{2+}$, $Ti(OH)_2^{+}$, $TiO_{2(s)}$ (anatase), $CaTiO_{3(s)}$, $Ti_2O_{3(s)}$, and $Ti_{(s)}$.*

the input molality of NH_3 on a logarithmic scale. In this case, pH is a dependent variable determined by the amount of NH_3 added to the solution. Figure 8 shows that CuO becomes thermodynamically unstable when the input amount of NH_3 reaches ~ 0.28 mol/kg. At equilibrium, this amount includes both $NH_{3(aq)}$ and NH_4^{+}.

In some cases, the chemical identity of passivation films can be influenced by changing the composition of the solution. This may occur when a sparingly soluble salt is thermodynamically more stable than a metal oxide. As shown in Figure 9, this

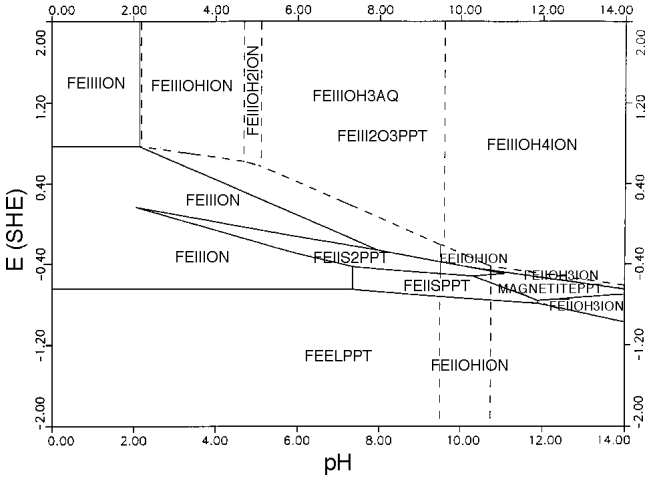

FIGURE 10. *Stability diagram for Fe in a 0.00001 molal H_2S solution with H_2SO_4 and NaOH used as pH-adjusting agents (T = 298.15 K, P = 1 bar). The symbols FEIIIION, FEIIIOHION, FEIIIOH2ION, FEIIIOH3AQ, FEIIIOH4ION, FEIIION, FEIIOHION, FEIIOH3ION, FEIIS2PPT, FEIISPPT, FEIII203PPT, MAGNETITEPPT, and FEELPPT denote Fe^{3+}, $FeOH^{2+}$, $Fe(OH)_2^+$, $Fe(OH)_{3(aq)}$, $Fe(OH)_4^-$, Fe^{2+}, $FeOH^+$, $Fe(OH)_3^-$, $FeS_{2(s)}$, $FeS_{(s)}$, $Fe_2O_{3(s)}$, $Fe_3O_{4(s)}$, and $Fe_{(s)}$.*

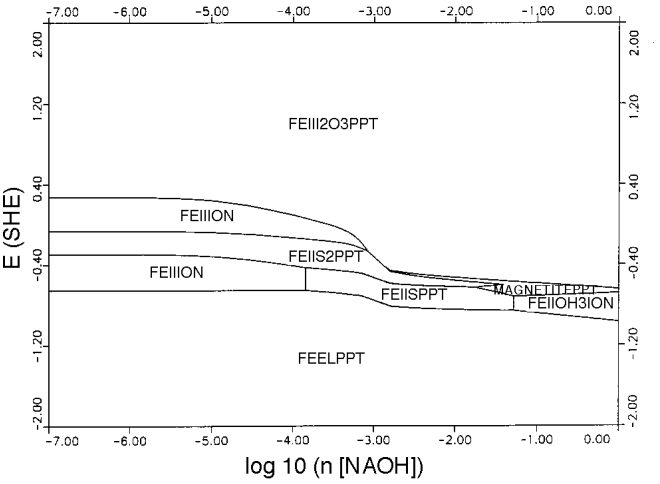

FIGURE 11. *Stability diagram for Fe in a 0.001 molal H_2S solution with a varying input amount of NaOH (from 10^{-7} to 1 mol/kg) at T = 298.15 K and P = 1 bar. The symbols FEIIION, FEIIOH3ION, FEIIS2PPT, FEIISPPT, FEIII2O3PPT, MAGNETITEPPT, and FEELPPT denote Fe^{2+}, $Fe(OH)_3^-$, $FeS_{2(s)}$, $FeS_{(s)}$, $Fe_2O_{3(s)}$, $Fe_3O_{4(s)}$, and $Fe_{(s)}$.*

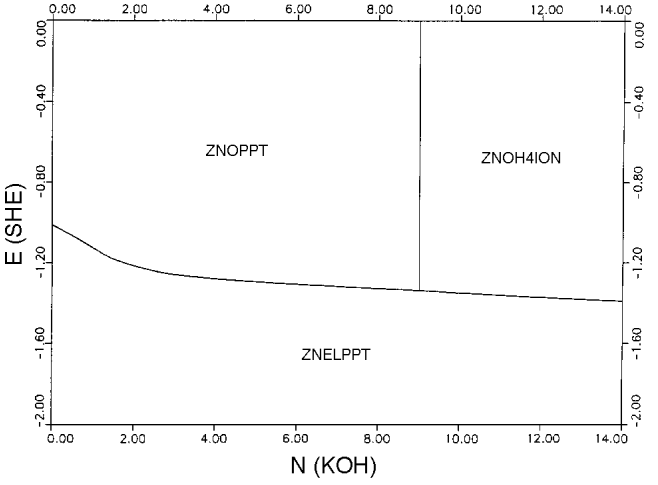

FIGURE 12. *Stability diagram for Zn in a system containing 1 mol ZnO, 1 kg H_2O, and varying amounts of KOH (from 0 to 14 mol). The symbols ZNOH4ION, ZNOPPT, and ZNELPPT denote $Zn(OH)_4^{2-}$, $ZnO_{(s)}$, and $Zn_{(s)}$.*

occurs in the case of titanium (Ti) in a solution that contains a small amount of calcium (Ca^{2+}) ions (i.e.. 0.01 mol/kg). Then, the titanium dioxide (TiO_2) passivating film becomes superseded by calcium titanate ($CaTiO_3$) at pH > 7.2. A Ti plate immersed in an alkaline solution containing Ca^{2+} ions will become covered with a $CaTiO_3$ layer. Since the H_2/H^+ line (a) intersects the stability field of $CaTiO_3$, this may occur in dearated and aerated solutions. The behavior of the Ti + Ca + H_2O system (Figure 9) provides a thermodynamic explanation for the preparation of thin films of $CaTiO_3$ on Ti anodes with or without an external electric field at temperatures ranging from 100°C to 300°C.[31] Similar syntheses have been reported for thin films of barium titanate ($BaTiO_3$) and strontium titanate ($SrTiO_3$), which have useful ferroelectric properties.[32]

Stability diagrams are particularly useful for predicting the behavior of metals in the presence of corrosive components such as H_2S.[6-8] In this work, stability diagrams are generated for Fe in the presence of a fixed amount of H_2S, which can be hydrolyzed with the formation of HS^- and S^{2-} ions or oxidized to $S_{(s)}^0$, SO_4^{2-}, or HSO_4^- (Figures 4 and 5). Figure 10 shows an E-vs-pH projection for Fe in a solution containing 10^{-5} mol H_2S in 1 kg of water. Since the solution is very dilute with respect to H_2S, Figure 10 is similar to the classical Pourbaix diagrams.[8] It is characteristic of a system in which the metal and the ligands (here, S^{2-}) are subject to oxidation-reduction reactions. For example, the stability range of pyrite (FeS_2) is enclosed partially by that of the Fe ions in weakly acidic solutions. The lower boundary of the FeS_2 area corresponds to the reductive dissolution of FeS_2 in which the disulfide ion S_2^{2-} is reduced to H_2S or HS^-. On the other hand, the upper boundary reflects the oxidative dissolution of FeS_2, which results in the oxidation of S_2^{2-} to HSO_4^-.

It is of interest to examine the behavior of this system as a function of the amount of a base that is used to neutralize H_2S to reduce the H_2S-induced acidic corrosion. Figure 11 shows the resulting diagram when the amount of H_2S is 10^{-3} mol/kg and the amount of NaOH varies from 10^{-7} to 1 mol/kg. A characteristic feature of this diagram is a small but

significant drop in the equilibrium potential of the Fe electrode when the amount of the added NaOH is ≈ 10^{-3} mol/kg. Such a drop is not observed on an E-vs-pH projection. It reflects the neutralization of H_2S and change in the concentration of the S^{2-} ions relative to the total amount of S in the –2 oxidation state. Projections of E vs the amount of a base added to a system are expected to be, in general, very useful because they correspond to a real-world situation when a base (or other reactant) is added to a working fluid. In such situations, pH is merely a resulting property and may not be convenient as an independent variable. Figure 11 shows the amount of the base for which the potentially protective FeS layer becomes stable. It also shows that the FeS phase ceases to be stable if more than ~ 0.05 mol/kg of NaOH is added. The stability field of the sulfide is followed by that of an aqueous species (i.e., $Fe[OH]_3^-$), which corresponds to corrosion in alkaline environments.

An important feature of the real-solution stability diagrams is their ability to represent the properties of metals in the presence of very concentrated solutions. This is because the thermodynamic model is capable of accurately reproducing solubility relations in concentrated solutions (up to ~ 30 mol/kg). Figure 12 shows the behavior of Zn in the presence of a system containing 1 mol of ZnO in 1 kg of H_2O in KOH solutions. This system is important for rechargeable battery applications. The input number of moles of KOH is varied from 0 to 14 mol. As the input amount of KOH increases, the potential of metallic Zn declines with most of the decrease occurring for relatively small amounts of KOH (up to 3 mol). The vertical line between ZnO and $Zn(OH)_4^{2-}$ corresponds to the solubility of ZnO. The amount of KOH that is needed to dissolve 1 mol of ZnO in a saturated solution closely agrees with the solubility data for the ternary system ZnO + KOH + H_2O.[29]

CONCLUSIONS

❖ A methodology was developed for combining the ease of use of the classical Pourbaix diagrams with a rigorous approach to modeling the thermodynamic properties of aqueous solutions.

❖ This methodology makes it possible to use comprehensive models for standard-state properties and activity coefficients in multicomponent solutions. Therefore, the resulting stability diagrams can be constructed for systems involving concentrated solutions (i.e., with ionic strengths up to 30 mol/kg) at T and P up to 573 K and 100 MPa, respectively

❖ An important feature of the real-solution stability diagrams is the possibility of using molalities (or mole numbers) rather than activities as independent variables. In the classical stability diagrams, it was impossible to decompose activities into concentrations and activity coefficients because of the absence of a model for activity coefficients in multicomponent solutions. Therefore, arbitrary values of activities had to be assumed for thermodynamic calculations. In the present approach, activity coefficients are calculated rigorously as functions of solution composition and temperature. Thus, only concentrations of input components are required as independent variables. Therefore, the predominance areas can be plotted as functions of concentrations in addition to pH. Thus, thermodynamic aspects of corrosion can be studied for metals in the presence of realistically modeled aqueous streams.

REFERENCES

1. M. Pourbaix, Atlas of Electrochemical Equilibria in Aqueous Solutions (New York, NY: Pergamon Press, 1966).
2. M.H. Froning, M.E. Shanley, E.D. Verink Jr., Corros. Sci. 16 (1976): p. 371.
3. C.M. Chen, K. Aral, Corrosion 38 (1982): p. 183.
4. J.C. Angus, C.T. Angus, J. Electrochem. Soc. 132 (1985): p. 1,014.
5. C.M. Criss, J.W. Cobble, J. Amer. Chem. Soc. 86 (1964): p. 5,385.
6. R.J. Biernat, R.G. Robbins, Electrochim. Acta 17 (1972): p. 1,261.
7. D.D. Macdonald, Corros. Sci. 16 (1976): p. 461.
8. D.D Macdonald, B.C. Syrett, Corrosion 35 (1979): p. 471.
9. D.D. Macdonald, P. Butler, Corros. Sci. 13 (1973): p. 259.
10. J.B. Lee, Corrosion 37 (1981): p. 467.
11. D.C. Silverman, Corrosion 38 (1982): p. 541.
12. G. Bianchi, P. Longhi, Corros. Sci. 13 (1973): p. 853.
13. J.F. Zemaitis Jr., D.M. Clark, M. Rafal, N.C. Scrivner, Handbook of Aqueous Electrolyte Thermodynamics (New York, NY: AIChE, 1986).
14. M. Rafal, J.W. Berthold, N.C. Scrivner, S.L. Grise, "Models for Electrolyte Solutions," in Models for Thermodynamic and Phase Equilibria Calculations, ed. S.I. Sandler (New York, NY: Marcel Dekker, 1995), p. 601.
15. H.C. Helgeson, D.H. Kirkham, Amer. J. Sci. 274 (1974): p. 1,089 and p. 1,199.
16. H.C. Helgeson, D.H. Kirkham, G.C. Flowers, Amer. J. Sci. 281 (1981): p. 1,249.
17. J.C. Tanger, H.C. Helgeson, Amer. J. Sci. 288 (1988): p. 19.
18. E.L. Shock, E.H. Oelkers, D.A. Sverjensky, J.W. Johnson, H.C. Helgeson, J. Chem. Soc. Faraday Trans. 88 (1992): p. 803.
19. E.L. Shock, H.C. Helgeson, Geochim. Cosmochim. Acta 52 (1988): p. 2,009.
20. E.L. Shock, H.C. Helgeson, Geochim. Cosmochim. Acta 54 (1990): p. 915.
21. E.L. Shock, H.C. Helgeson, D.A. Sverjensky, Geochim. Cosmochim. Acta 53 (1989): p. 2,157.
22. D.A. Sverjensky, in Reviews in Mineralogy, eds. I.S.E. Carmichael, H.P. Eugster, vol. 17 (Washington, DC: Mineralogical Society of America, 1987).
23. L.A. Bromley, J. Chem. Thermodyn. 4 (1972): p. 669.
24. L.A. Bromley, AIChE J. 19 (1973): p. 313.
25. P. Debye, E. Huckel, Physik. Z. 24 (1923): p. 185.
26. H.P. Meissner, AIChE Symp. Ser. 173 (1978): p. 74.
27. K.S. Pitzer, J. Phys. Chem. 77 (1973): p. 268.
28. T.M. Smolen, D.B. Manley, B.E. Poling, J. Chem. Eng. Data 36 (1991): p. 202.
29. T.P. Dirkse, J. Electrochem. Soc. 106 (1959): p. 154.
30. M.J. Isaacson, F.R. McLarnon, E.J. Cairns, J. Electrochem. Soc. 137 (1990): p. 2,361.
31. Y. Sakabe, Y. Hamaji, M. Hayashi, Y. Ogino, N. Ishizawa, M. Yoshimura, "Synthesis of $SrTiO_3$ and $CaTiO_3$ Thin Films by Hydrothermal Electrochemical Method," paper no. IV-7, in Proc. 5th U.S.-Japan Seminar on Dielectric and Piezoelectric Ceramics (Kyoto, Japan: Japanese Ceramic Society, 1990), p. 300.
32. M. Yoshimura, S.E. Yoo, M. Hayashi, N. Ishizawa, Jpn. J. Appl. Phys. 2 (1989): p. L2,007.